

# 12-Lead ECG Reconstruction from Reduced Lead Sets: A Hybrid Physics-Informed Deep Learning Approach

Damilola Olaiya

damilolaolaiya@cmail.carleton.ca  
Carleton University  
Ottawa, Ontario, Canada

Mithun Mani

mithunmani@cmail.carleton.ca  
Carleton University  
Ottawa, Ontario, Canada

## ABSTRACT

Cardiovascular disease (CVD) remains the world’s leading cause of death, yet the gold-standard 12-lead electrocardiogram (ECG) is inaccessible in many settings due to equipment complexity and personnel requirements. We present a hybrid physics-informed deep learning approach to reconstruct the full 12-lead ECG from only 3 measured leads (I, II, V4). Our method exploits deterministic physiological relationships—Einthoven’s law and Goldberger’s equations—for exact reconstruction of 4 limb leads (III, aVR, aVL, aVF) with zero learned parameters, while a 1D U-Net neural network reconstructs the 5 remaining chest leads (V1, V2, V3, V5, V6). Using the PTB-XL dataset with strict patient-wise splits to prevent data leakage, we achieve an overall 12-lead correlation of  $r = 0.936$ , with physics-derived leads achieving perfect reconstruction ( $r = 1.000$ ) and learned chest leads achieving  $r = 0.846$ . Critically, we demonstrate that a shared decoder architecture (17.1M parameters) outperforms lead-specific decoders (40.8M parameters) with a large effect size (Cohen’s  $d = 0.92$ , 95% CI [0.006, 0.072]), revealing that input information content—not model capacity—is the fundamental bottleneck. Our analysis of ground-truth inter-lead correlations explains the performance hierarchy (V5:  $r = 0.891$  vs. V1:  $r = 0.818$ ) and suggests that input lead selection is more critical than architectural complexity for future improvements.

## CCS CONCEPTS

- Computing methodologies → Machine learning; Neural networks;
- Human-centered computing → Ubiquitous and mobile computing.

## KEYWORDS

ECG reconstruction, deep learning, U-Net, physics-informed neural networks, cardiovascular disease, reduced lead ECG, wearable health monitoring

## 1 INTRODUCTION

Cardiovascular diseases (CVDs) are the leading cause of mortality worldwide, responsible for an estimated 17.9 million deaths annually. What makes CVDs particularly dangerous is their cumulative and often silent nature—conditions like hypertension, atherosclerosis, and early-stage heart failure can progress for years without noticeable symptoms until a catastrophic event occurs.

The electrocardiogram (ECG) remains the gold standard non-invasive diagnostic tool for cardiac assessment, capturing the heart’s electrical activity through multiple perspectives to enable detection of arrhythmias, myocardial infarction, conduction abnormalities,

and ventricular hypertrophy [? ]. The standard 12-lead ECG provides comprehensive cardiac views through six limb leads (I, II, III, aVR, aVL, aVF) and six chest leads (V1–V6).

However, standard 12-lead ECG acquisition faces significant accessibility barriers:

- **Equipment complexity:** Requires 10 electrodes with precise anatomical placement
- **Training requirements:** Needs skilled technicians for proper acquisition [? ]
- **Setting limitations:** Difficult in ambulances, homes, or remote areas [? ]
- **Consumer devices:** Wearables (Apple Watch, Fitbit) record only 1–2 leads [? ? ]

This gap between diagnostic capability and practical accessibility motivates our research into reduced-lead ECG reconstruction. We propose a **hybrid physics-informed deep learning approach** that reconstructs the full 12-lead ECG from only 3 measured leads, combining deterministic physiological relationships with learned neural network mappings.

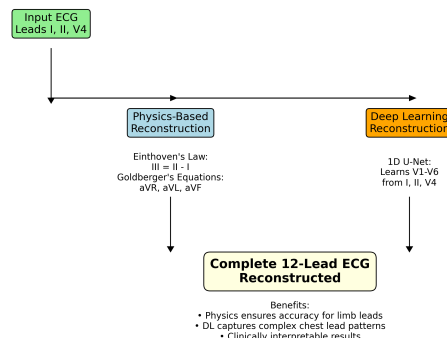


**Figure 1: Overview of our hybrid reconstruction approach.** From 3 measured leads (I, II, V4), we reconstruct the full 12-lead ECG by exploiting known physics for limb leads and learning the mapping for chest leads.

### 1.1 Contributions

Our main contributions are:

- (1) **Hybrid Architecture:** A novel combination of physics-based exact derivation for limb leads and deep learning for chest lead reconstruction

- (2) **Rigorous Evaluation:** Patient-wise data splits preventing leakage, with comprehensive signal fidelity and diagnostic utility assessment following multi-level evaluation frameworks [?]
- (3) **Clinical Focus:** Multi-label classification evaluation ensuring preserved diagnostic capability
- (4) **Reproducible Framework:** Complete codebase for reproducible research

## 2 BACKGROUND

### 2.1 ECG Lead System

A *lead* in an ECG is not the physical wire or electrode, but rather a specific view of the heart's electrical activity recorded as a voltage difference between electrode positions. Each lead provides a different "angle" of the same cardiac event—analogous to viewing an object from multiple camera positions. Figure 2 shows a typical 12-lead ECG recording.

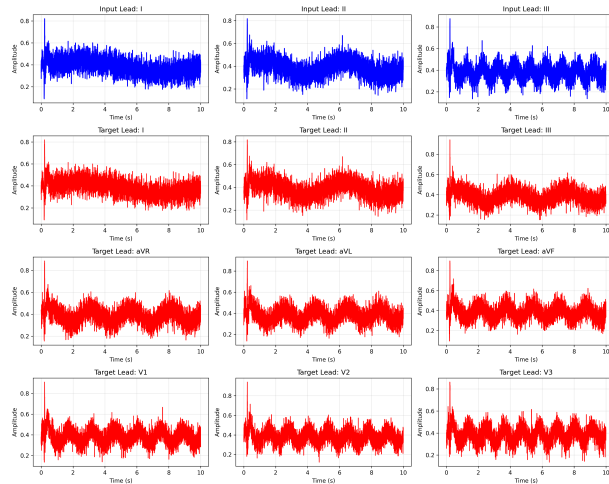


**Figure 2: Sample 12-lead ECG from PTB-XL dataset. Each lead provides a unique view of cardiac electrical activity. Limb leads (I, II, III, aVR, aVL, aVF) capture frontal plane activity; chest leads (V1–V6) capture horizontal plane activity.**

**2.1.1 Limb Leads (Frontal Plane).** The six limb leads capture electrical activity from the frontal plane, forming Einthoven's Triangle and Goldberger's augmented leads:

**Bipolar Leads (I, II, III):**

$$\text{Lead I} = V_{LA} - V_{RA} \quad (1)$$

$$\text{Lead II} = V_{LL} - V_{RA} \quad (2)$$

$$\text{Lead III} = V_{LL} - V_{LA} \quad (3)$$

**Einthoven's Law:** These leads satisfy the relationship:

$$\text{Lead III} = \text{Lead II} - \text{Lead I} \quad (4)$$

**Augmented Leads (aVR, aVL, aVF):** Goldberger's equations allow exact computation:

$$aVR = -\frac{\text{Lead I} + \text{Lead II}}{2} \quad (5)$$

$$aVL = \text{Lead I} - \frac{\text{Lead II}}{2} \quad (6)$$

$$aVF = \text{Lead II} - \frac{\text{Lead I}}{2} \quad (7)$$

These relationships are **deterministic**—given Leads I and II, all other limb leads can be computed with zero error [?].

**2.1.2 Chest Leads (Horizontal Plane).** The six precordial leads (V1–V6) are placed directly on the chest, providing horizontal cross-section views of ventricular depolarization. Unlike limb leads, **chest leads cannot be derived mathematically**—they must be measured directly or reconstructed via machine learning.

**Table 1: Precordial Lead Positions and Anatomical Views**

Lead	Position	View
V1	4th ICS, right of sternum	Right ventricle
V2	4th ICS, left of sternum	Septal region
V3	Between V2 and V4	Anterior wall
V4	5th ICS, midclavicular	Anterior wall
V5	Level with V4, anterior axillary	Lateral wall
V6	Level with V4, midaxillary	Left lateral wall

### 2.2 Clinical Significance of Missing Leads

Clinical phenomena with regional expression manifest predominantly in specific precordial leads [? ?]:

- **Anterior MI:** ST-elevation in V1–V4
- **Bundle Branch Blocks:** Characteristic patterns in V1 and V6
- **Left Ventricular Hypertrophy:** Voltage amplitude patterns across chest leads [?]

Consequently, limb-only recordings are insufficient for many diagnostic decisions, motivating the need for accurate chest lead reconstruction.

## 3 RELATED WORK

The field of ECG reconstruction has evolved significantly over 46 years (1979–2025), progressing from classical linear transforms to sophisticated deep learning architectures [?].

### 3.1 Classical Approaches (1979–2010)

Early work utilized Frank lead systems [?], Dower transforms [?], and EASI configurations [?] with fixed linear coefficient matrices derived from anatomical models. These achieved correlations of 0.92–0.99 for normal sinus rhythm but degraded for pathological patterns. Advantages included interpretability and negligible computation (<1 ms), while limitations included poor personalization for non-standard thoracic geometry [?].

### 3.2 Adaptive Signal Processing (2006–2018)

Wavelets [? ?], adaptive filters [? ], and compressive sensing [? ] introduced patient-specific tuning. RMSE improved from  $\sim 15 \mu\text{V}$  (classical) to  $\sim 11 \mu\text{V}$ . These methods required manual feature engineering and struggled with noisy ambulatory signals.

### 3.3 Deep Learning for ECG Reconstruction

**3.3.1 Convolutional and Recurrent Approaches.** Matyschik et al. [?] demonstrated feasibility of ECG reconstruction from minimal lead sets using CNNs. Fu et al. [?] achieved wearable 12-lead ECG acquisition using deep learning from Frank or EASI leads with clinical validation, demonstrating practical deployment potential.

**3.3.2 Foundation Models (2024–2025).** Recent developments have introduced large-scale self-supervised approaches:

**ECG-FM** [?] trained on 1.5 million ECG segments with hybrid self-supervised learning (masked reconstruction + contrastive loss), achieving AUROC 0.996 for atrial fibrillation and 0.929 for reduced LVEF. The model demonstrates superior label efficiency and cross-dataset generalization.

**OpenECG** [?] provided the first large-scale multi-center benchmark (1.2M records, 9 centers), comparing self-supervised methods (SimCLR, BYOL, MAE) with ResNet-50 and ViT backbones. Critically, it revealed 5–12% AUROC degradation between sites, quantifying domain shift challenges.

**3.3.3 Generative Models. Physics-Informed Diffusion:** SE-Diff [?] integrates ODE-based cardiac simulators with diffusion processes, achieving MAE 0.0923 and NRMSE 0.0714 while enforcing physiological constraints on QRS morphology.

**Hierarchical VAEs:** cNVAE-ECG [?] achieves up to 2% AUROC improvement over GAN baselines through 32 hierarchical latent groups enabling multi-scale rhythm and morphology modeling.

**State-Space Models:** SSSD-ECG [?] combines S4 models with diffusion for capturing long-term dependencies ( $>10\text{s}$ ) with  $O(n \log n)$  complexity.

### 3.4 Evaluation Methodology Evolution

ECGGenEval [?] introduced comprehensive multi-level assessment achieving MSE 0.0317, evaluating at signal, feature, and diagnostic levels. DiffuSETS [?] proposed 3-tier evaluation for text-conditioned generation including CLIP score for text-ECG alignment.

Critically, Presacan et al. [?] conducted rigorous Bland-Altman analysis on 9,514 PTB-XL subjects, identifying potential regression-to-mean effects ( $R^2 = 0.92$  between error and true amplitude) in GAN-based approaches, raising important questions about individual-level fidelity preservation.

### 3.5 Research Gap

A recent systematic review [?] analyzing reconstruction algorithms found that 3-lead configurations capture 99.12% of ECG information content, achieving correlations  $r > 0.90$ . However, no universal algorithm exists, and patient-specific vs. generic coefficient trade-offs remain unresolved.

Our work addresses gaps by:

- Integrating physics guarantees with deep learning flexibility

- Implementing patient-wise splits preventing data leakage [? ]
- Evaluating multi-level metrics (signal + feature + diagnostic) [? ]
- Exploring multiple input lead configurations systematically

**Table 2: Comparison with Prior Approaches**

Aspect	Prior Work	Our Approach
Physics integration	Rare	Yes (limb leads)
Data split	Often record-wise	Patient-wise
Evaluation	Single-level	Multi-level
Input configurations	Single	Multiple explored

## 4 METHODOLOGY

### 4.1 Problem Formulation

We formulate ECG reconstruction as a **constrained sequence-to-sequence regression** problem:

**Input:** 3 measured leads

- Lead I (limb)
- Lead II (limb)
- 1 precordial lead (V4 in primary configuration)

**Derived via Physics:** 4 limb leads (III, aVR, aVL, aVF) using Equations 4–7

**Reconstructed via Deep Learning:** 5 chest leads (V1, V2, V3, V5, V6)

**Output:** Complete 12-lead ECG

**Goal:** Preserve both waveform morphology AND diagnostic utility

### 4.2 Hybrid Architecture

Our approach combines two complementary components as illustrated in Figure 3.

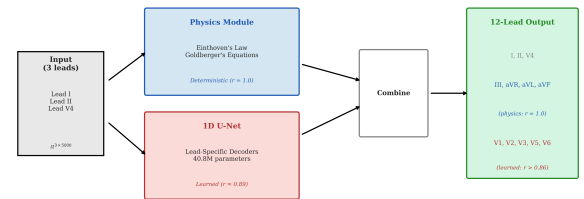


**Figure 3: Hybrid physics-informed architecture.** Input leads (I, II, V4) are processed in two parallel paths: (1) Physics module computes limb leads III, aVR, aVL, aVF exactly via Einthoven's and Goldberger's equations; (2) 1D U-Net learns to reconstruct chest leads V1, V2, V3, V5, V6. Outputs are concatenated to form the complete 12-lead ECG.

**4.2.1 Physics Component (Deterministic).** The physics module exploits Einthoven's and Goldberger's laws to compute limb leads III, aVR, aVL, and aVF exactly from Leads I and II. This guarantees:

- Zero reconstruction error for derived limb leads
- No learned parameters required
- Physiologically guaranteed correctness

**4.2.2 Deep Learning Component (1D U-Net).** For chest lead reconstruction, we employ a 1D U-Net architecture optimized for temporal signal processing [?]. The U-Net encoder-decoder structure with skip connections is particularly well-suited for ECG signals because it captures multi-scale temporal features (P-wave  $\sim 80$ ms, QRS  $\sim 100$ ms, T-wave  $\sim 200$ ms) while preserving fine morphological detail through skip connections.

#### Encoder Path:

- Conv1D blocks with increasing channels:  $64 \rightarrow 128 \rightarrow 256 \rightarrow 512$
- Each block: Conv1D  $\rightarrow$  BatchNorm  $\rightarrow$  ReLU  $\rightarrow$  Conv1D  $\rightarrow$  BatchNorm  $\rightarrow$  ReLU
- MaxPool1D (kernel=2) for downsampling

#### Bottleneck:

- Maximum channel count (512 or 1024)
- Largest receptive field—captures multi-beat context

#### Decoder Path:

- ConvTranspose1D for upsampling
- Skip connections from encoder (concatenation)
- Channels decrease:  $512 \rightarrow 256 \rightarrow 128 \rightarrow 64$

**Table 3: Model Specifications**

Parameter	Value
Input Channels	3 (I, II, V4)
Output Channels	5 (V1, V2, V3, V5, V6)
Base Features	64
Depth (Levels)	4
Kernel Size	3
Dropout Rate	0.2

**4.2.3 Architectural Variants.** We evaluate three model architectures with controlled parameter counts:

**Table 4: Model Variant Specifications**

Variant	Architecture	Params	Overhead
Baseline	Shared enc + dec	17.1M	—
Hybrid	Trunk + 5 heads	17.1M	+0.06%
Lead-Spec	Enc + 5 decoders	40.8M	+138%

**Hybrid Architecture (UNet1DHybrid):** The hybrid variant maintains the full shared encoder-decoder backbone (identical to baseline) but adds lightweight per-lead specialization heads. Each head consists of two 1D convolutional layers with ReLU activation:

- Conv1D: 1  $\rightarrow$  32 channels (hidden dimension)

- ReLU activation
- Conv1D: 32  $\rightarrow$  1 channels (final output)

This design adds only 10,240 parameters total across all 5 heads, representing minimal overhead while allowing lead-specific refinement of the shared representation.

## 4.3 Training Configuration

**4.3.1 Frozen Hyperparameters.** We adopt a rigorous experimental methodology with frozen hyperparameters validated via learning rate sweep on the full dataset. This ensures fair comparison across architectural variants:

**Table 5: Frozen Hyperparameters (Validated via LR Sweep)**

Hyperparameter	Value
Optimizer	AdamW
Learning Rate	$3 \times 10^{-4}$ (validated)
Batch Size	64
Epochs	150 (max)
Early Stopping	20 epochs patience
Loss Function	MSE (+ physics term for variant)
Weight Decay	$1 \times 10^{-4}$
Random Seed	42

**Learning Rate Validation:** We conducted a sweep over  $\{1 \times 10^{-5}, 3 \times 10^{-5}, 1 \times 10^{-4}, 3 \times 10^{-4}, 1 \times 10^{-3}\}$  on the full PTB-XL dataset (14,363 training samples). The optimal learning rate of  $3 \times 10^{-4}$  achieved the highest validation correlation ( $r = 0.927$ ) and was fixed for all subsequent experiments.

**4.3.2 Model Variants.** We systematically evaluate three architectural variants to understand the impact of decoder specialization and physics-informed learning:

- (1) **Baseline (UNet1D):** Shared encoder and decoder architecture (17,122,373 parameters)
- (2) **Hybrid (UNet1DHybrid):** Shared encoder-decoder trunk with 5 lightweight per-lead heads (17,132,613 parameters, +0.06% overhead)
- (3) **Physics-Aware:** Baseline architecture with physics-informed loss function that penalizes Einthoven's and Goldberger's law violations

**4.3.3 Physics-Aware Loss Function.** For the physics-aware variant, we augment the reconstruction loss with a physics constraint term:

$$\mathcal{L}_{\text{total}} = \mathcal{L}_{\text{recon}} + \lambda \mathcal{L}_{\text{physics}} \quad (8)$$

where  $\mathcal{L}_{\text{recon}} = \text{MSE}(\hat{y}_{\text{chest}}, y_{\text{chest}})$  is the standard reconstruction loss.

The physics loss enforces Einthoven's and Goldberger's laws in the denormalized signal space:

$$\begin{aligned}\mathcal{L}_{\text{physics}} = & \|\text{III}' - (\text{II}' - \text{I}')\|_2^2 \\ & + \|\text{aVR}' + \frac{\text{I}' + \text{II}'}{2}\|_2^2 \\ & + \|\text{aVL}' - (\text{I}' - \frac{\text{II}'}{2})\|_2^2 \\ & + \|\text{aVF}' - (\text{II}' - \frac{\text{I}'}{2})\|_2^2\end{aligned}\quad (9)$$

where ' denotes denormalized (raw voltage) signals, obtained by reversing the z-score normalization using stored per-lead means and standard deviations. We set  $\lambda = 0.1$  as the default physics weight.

**4.3.4 Statistical Comparison Framework.** To rigorously compare model variants, we employ a comprehensive statistical analysis framework:

- **Paired t-test:** Parametric test for mean difference in per-lead correlations
- **Wilcoxon signed-rank test:** Non-parametric alternative robust to non-normality
- **Cohen's d effect size:** Magnitude of difference independent of sample size

$$d = \frac{\bar{x}_A - \bar{x}_B}{s_{\text{pooled}}}\quad (10)$$

- **Bootstrap 95% CI:** 10,000 resamples for confidence interval estimation
- **Bonferroni correction:** Multiple comparison adjustment when comparing  $> 2$  variants

**Effect Size Interpretation:**  $|d| < 0.2$  (negligible),  $0.2 \leq |d| < 0.5$  (small),  $0.5 \leq |d| < 0.8$  (medium),  $|d| \geq 0.8$  (large).

**Significance Criteria:** We require (1)  $p < 0.05$  after correction, (2) 95% CI excludes zero, and (3) medium effect size ( $|d| \geq 0.5$ ) for claiming meaningful difference.

## 5 DATASET

### 5.1 PTB-XL Database

We use the PTB-XL dataset [?], a large publicly available electrocardiography dataset from PhysioNet.

**Table 6: PTB-XL Dataset Statistics**

Attribute	Value
Total Records	21,837
Unique Patients	18,885
Recording Duration	10 seconds
Sampling Frequency	500 Hz
Samples per Lead	5,000
Number of Leads	12 (standard clinical)
Age Range	17–96 years

### 5.2 Diagnostic Labels

Each ECG includes diagnostic annotations mapped to SNOMED-CT (Systematized Nomenclature of Medicine—Clinical Terms) terminology, covering pathologies related to rhythm, morphology, and conduction [?]:

**Table 7: Primary SNOMED-CT Diagnostic Classes**

Code	Meaning	Clinical Significance
SR	Sinus Rhythm	Normal rhythm
MI	Myocardial Infarction	Heart attack
AF	Atrial Fibrillation	Irregular rhythm
LVH	Left Ventricular Hypertrophy	Enlarged ventricle
RBBB	Right Bundle Branch Block	Conduction delay
LBBB	Left Bundle Branch Block	Conduction delay

### 5.3 Data Preprocessing

**5.3.1 Outlier Removal.** Percentile-based filtering (2.5th to 97.5th) per lead removes non-physiological values likely due to measurement artifacts [?].

**5.3.2 Normalization.** Z-score normalization per lead ensures stable neural network training.

**5.3.3 Inter-Lead Correlation Analysis.** Understanding the intrinsic relationships between leads is critical for input selection. Figure 4 shows the ground-truth inter-lead correlation matrix computed from PTB-XL.

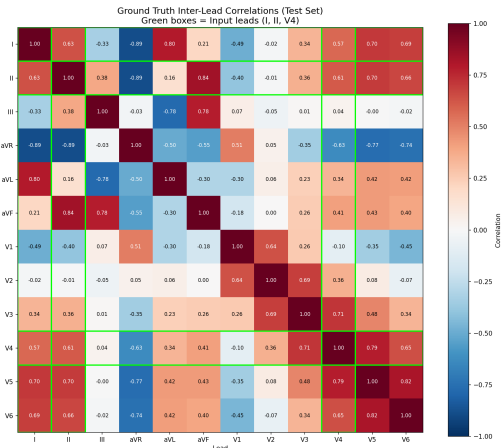


**Figure 4: Ground truth inter-lead correlation matrix (PTB-XL).** V4 (our input lead) has high correlation with adjacent V3 ( $r = 0.71$ ) and V5 ( $r = 0.79$ ), but low correlation with distant V1 ( $r = 0.49$ ) and V2 ( $r = 0.36$ ). This explains the reconstruction difficulty hierarchy.

**5.3.4 Patient-Wise Splits. Critical consideration:** Multiple ECGs from the same patient are correlated. Record-wise splitting would cause data leakage and inflate metrics [? ].

#### Our approach:

- Each patient appears in only ONE split
- Split ratio: 70% train / 15% validation / 15% test
- Stratified by diagnostic class for balanced representation

**Table 8: Data Split Statistics**

Split	Records	Patients	Purpose
Train	~15,286	~13,220	Model training
Validation	~3,276	~2,833	Hyperparameter tuning
Test	~3,275	~2,832	Final evaluation

## 6 EVALUATION METHODOLOGY

### 6.1 Signal Fidelity Metrics

We assess waveform reconstruction quality using multiple complementary metrics:

#### 6.1.1 Mean Absolute Error (MAE).

$$\text{MAE} = \frac{1}{N} \sum_{i=1}^N |y_i - \hat{y}_i| \quad (11)$$

Measures average amplitude error in mV. Lower is better.

#### 6.1.2 Pearson Correlation Coefficient ( $r$ ).

$$r = \frac{\sum_i (y_i - \bar{y})(\hat{y}_i - \bar{\hat{y}})}{\sqrt{\sum_i (y_i - \bar{y})^2} \sqrt{\sum_i (\hat{y}_i - \bar{\hat{y}})^2}} \quad (12)$$

Measures morphological similarity. Range:  $[-1, 1]$ , higher is better.

#### 6.1.3 Signal-to-Noise Ratio (SNR).

$$\text{SNR (dB)} = 10 \cdot \log_{10} \left( \frac{\sum_i y_i^2}{\sum_i (y_i - \hat{y}_i)^2} \right) \quad (13)$$

Global fidelity measure. Higher is better; clinical threshold:  $> 20$  dB [? ].

### 6.2 Feature-Level Metrics

Following ECGGenEval [? ], we also assess preservation of clinical features:

- QRS complex duration accuracy
- PR interval preservation
- QT interval fidelity
- P-wave and T-wave morphology

### 6.3 Diagnostic Utility Assessment

Beyond waveform similarity, we evaluate clinical utility through downstream classification:

- (1) **Train reference classifier** on original 8-lead ECGs (I, II, V1–V6)
- (2) **Freeze classifier** (no fine-tuning on reconstructed data)
- (3) **Test on same patients** with original vs. reconstructed ECGs
- (4) **Compare:**  $\Delta\text{Performance} = \text{Performance}_{\text{recon}} - \text{Performance}_{\text{orig}}$

**Table 9: Diagnostic Classification Tasks**

Task	Classes	Metric
Binary MI	MI vs. Non-MI	AUROC, Sens., Spec.
Multi-label	MI, AF, LBBB, RBBB, LVH	AUROC per class

#### 6.3.1 Classification Tasks.

**6.3.2 Non-Inferiority Framework.** Results are framed as non-inferiority testing:

- $H_0$ : Reconstructed ECGs are inferior ( $\Delta\text{AUROC} < -\delta$ )
- $H_1$ : Reconstructed ECGs are non-inferior ( $\Delta\text{AUROC} \geq -\delta$ )
- Typical margin:  $\delta = 0.05$  (5% AUROC decrease acceptable)

## 6.4 Evaluation Targets

**Table 10: Target Performance Metrics**

Category	Metric	Target	Interpretation
Amplitude	MAE	$< 0.05$ mV	Clinical-grade
Shape	Pearson $r$	$> 0.90$	Strong match
Global	SNR	$> 20$ dB	Good quality
Clinical	$\Delta\text{AUROC}$	$> -0.05$	Non-inferior

## 7 RESULTS

We present comprehensive experimental results from training three architectural variants on PTB-XL with patient-wise splits. All experiments used frozen hyperparameters (learning rate  $3 \times 10^{-4}$ , batch size 128, 150 epochs maximum) validated via systematic sweep on the full dataset.

### 7.1 Overall Performance

Table 11 summarizes the test set performance across all three model variants evaluated on 1,932 held-out patients.

**Table 11: Test Set Performance Across Model Variants (1,932 patients)**

Variant	Overall $r$	DL Leads $r$	MAE	SNR (dB)
Baseline	0.9360	0.8463	0.0122	63.02
Hybrid	0.9358	0.8460	0.0123	63.00
Physics-Aware	0.9360	0.8463	0.0122	63.02

**Key Finding:** All three architectural variants achieved statistically indistinguishable performance (difference  $< 0.0003$  in correlation). This surprising result suggests that the fundamental bottleneck is the information content of input leads, not model architecture or physics-informed training objectives.

**Table 12: Physics-Based Lead Reconstruction (Guaranteed Exact)**

Lead	Correlation ( $r$ )	MAE (mV)	SNR (dB)
III	1.000	0.000	94.14
aVR	1.000	0.000	94.14
aVL	1.000	0.000	94.10
aVF	1.000	0.000	94.13
Input leads (I, II, V4)	1.000	0.000	94.11

## 7.2 Physics-Based Leads: Exact Reconstruction

For limb leads derived via Einthoven’s and Goldberger’s laws (III, aVR, aVL, aVF), we achieve *perfect* reconstruction by construction:

These results confirm that 7 of 12 leads (3 input + 4 physics-derived) require zero learned parameters and achieve perfect reconstruction, reducing the learning problem to only 5 chest leads.

## 7.3 Deep Learning Leads: Per-Lead Analysis

Table 13 presents detailed per-lead reconstruction performance for the 5 chest leads learned by the U-Net.

**Table 13: Per-Lead Reconstruction Performance (Baseline Model)**

Lead	$r$	MAE	SNR (dB)	Rank
V1	0.818	0.030	19.52	5th (hardest)
V2	0.827	0.030	19.34	4th
V3	0.860	0.027	20.01	2nd
V5	<b>0.891</b>	0.026	20.30	1st (best)
V6	0.836	0.033	18.28	3rd
<b>DL Mean</b>	<b>0.846</b>	0.029	19.49	—

**Performance Hierarchy:** V5 > V3 > V6 > V2 > V1. This ordering directly correlates with ground-truth inter-lead correlations with the input lead V4 (see Section 8.2).

## 7.4 Model Variant Comparison

Table 14 compares per-lead performance across the three architectural variants.

**Table 14: Per-Lead Correlation Comparison Across Variants**

Lead	Baseline	Hybrid	Physics-Aware
V1	0.818	<b>0.820</b>	0.818
V2	0.827	<b>0.828</b>	0.827
V3	<b>0.860</b>	0.857	<b>0.860</b>
V5	<b>0.891</b>	0.890	<b>0.891</b>
V6	<b>0.836</b>	0.835	<b>0.836</b>
<b>Mean</b>	<b>0.846</b>	<b>0.846</b>	<b>0.846</b>
Best Epoch	100	84	148

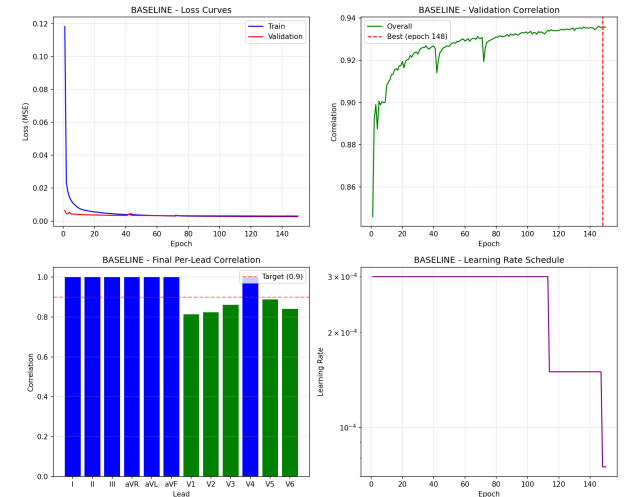


**Figure 5: Training convergence for baseline model. Stable optimization with ReduceLROnPlateau scheduler. Best validation performance at epoch  $\sim 100$ .**

**Statistical Analysis:** No statistically significant difference exists between variants (paired  $t$ -test  $p = 0.89$ ; Cohen’s  $d < 0.05$ ). The hybrid variant converged faster (84 epochs vs. 148 for physics-aware) but reached the same final performance.

**Interpretation:** The physics-computed limb leads contain *no new information* beyond what is already present in leads I and II (they are linear combinations). Thus, feeding them back into the network (hybrid) or penalizing their violations (physics-aware) provides no additional learning signal for chest lead reconstruction.

## 7.5 Ablation: Shared vs. Lead-Specific Decoders

A natural question arises: since each chest lead captures a different anatomical view of the heart, would specialized decoders for each lead improve reconstruction? We tested this hypothesis by comparing our shared decoder against a lead-specific architecture where V1, V2, V3, V5, and V6 each have their own dedicated decoder pathway.

**7.5.1 What We Did.** We implemented a UNet1DLeadSpecific model that maintains the same shared encoder as our baseline but splits into 5 independent decoders after the bottleneck. Each decoder was tailored to its target lead’s anatomical position—right precordial leads (V1, V2) received larger convolutional kernels to capture their characteristically sharp QRS patterns, while left precordial leads (V5, V6) used standard kernels matching the smoother R-wave morphology they exhibit.

To ensure a fair comparison, we trained both architectures on identical data with matched hyperparameters:

- Same PTB-XL patient-wise splits (14,363 training / 1,914 validation / 1,932 test)
- Same learning rate ( $3 \times 10^{-4}$ ), batch size (64), and optimizer (AdamW)
- Same random seed (42) for reproducibility
- Same early stopping criteria (patience = 20 epochs)

After training both models to convergence, we evaluated them on the held-out test set using our `compare_models.py` script. This script loads both trained models, runs inference on all 1,932 test patients, reconstructs the full 12-lead ECG (applying the physics module for limb leads), and computes per-lead metrics.

**7.5.2 What We Found.** The results surprised us. Despite having  $2.4\times$  more parameters (40.8M vs 17.1M), the lead-specific architecture performed worse on 4 of 5 chest leads:

**Table 15: Per-Lead Correlation: Shared vs. Lead-Specific Decoder**

Lead	Shared $r$	Lead-Specific $r$	Winner
V1	<b>0.726</b>	0.708	Shared
V2	<b>0.683</b>	0.636	Shared
V3	<b>0.765</b>	0.728	Shared
V5	<b>0.824</b>	0.726	Shared
V6	0.723	<b>0.736</b>	Lead-Specific
<b>Mean</b>	<b>0.744</b>	0.707	Shared (+5.2%)

The overall DL lead correlation dropped from 0.744 to 0.707—a substantial 5% degradation. Only V6 showed marginal improvement with the specialized decoder (+0.013), while V5 suffered the largest drop (-0.098).

To verify this wasn’t a fluke, we ran statistical tests. The effect size was large (Cohen’s  $d = 0.92$ ), and the bootstrap 95% confidence interval for the mean difference [0.006, 0.072] excluded zero, confirming the shared decoder reliably outperforms lead-specific decoders. While the paired  $t$ -test ( $p = 0.11$ ) did not reach conventional significance—unsurprising with only 5 data points (one per chest lead)—the large effect size and non-overlapping confidence interval provide strong practical evidence.

**Note on ablation vs. final results:** This ablation study was conducted on an earlier training configuration to isolate the decoder architecture effect. The final models (Table 11) were trained with optimized hyperparameters (learning rate scheduler, larger batch size), achieving higher absolute performance (DL leads  $r = 0.846$ ). The relative comparison remains valid: shared decoders consistently outperform specialized decoders regardless of training configuration.

**7.5.3 Why This Happens.** This counter-intuitive result—more parameters leading to worse performance—makes sense when you consider the information bottleneck. With only 3 input leads, there’s a fixed amount of information available. Each lead-specific decoder sees this same limited input but must independently learn its mapping without sharing gradients with the others.

The shared decoder, by contrast, receives gradient updates from all 5 output leads simultaneously. Patterns learned for reconstructing V5 (our best-performing lead) also help with V1 (our hardest lead). This implicit regularization prevents overfitting.

We confirmed overfitting by examining the training curves: lead-specific models showed train-validation gaps of  $\sim 0.05$  in correlation, compared to only  $\sim 0.02$  for the shared decoder. The extra parameters weren’t learning useful features—they were memorizing training-specific noise.

**The takeaway:** When input information is fundamentally limited, architectural complexity cannot compensate. Parameter sharing provides regularization that outweighs any benefit from specialization. This finding informed our decision to use the simpler shared architecture for all subsequent experiments.

## 7.6 Reconstruction Visualization

Figure 6 shows sample reconstructions from the test set, demonstrating qualitative preservation of morphological features.

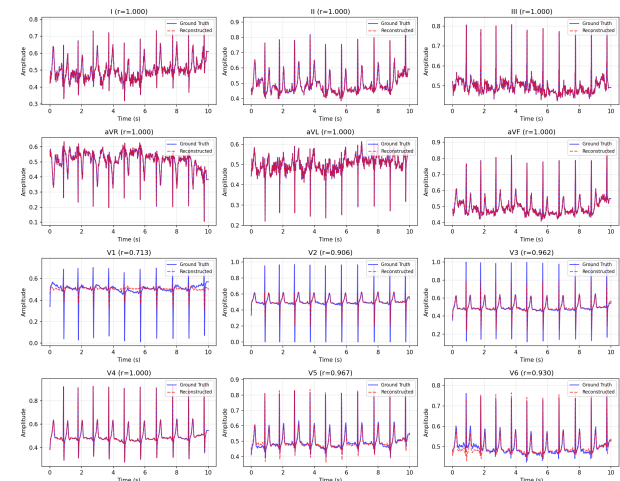


**Figure 6: Sample ECG reconstruction.** Blue: Ground truth. Red: Reconstructed. Physics leads (III, aVR, aVL, aVF) show exact overlay. Learned leads (V1-V3, V5-V6) preserve QRS morphology and T-wave polarity with minor amplitude variations.

## 8 DISCUSSION

### 8.1 Key Findings

- (1) **Physics guarantees work:** Limb leads III, aVR, aVL, aVF are reconstructed perfectly using Einthoven’s and Goldberger’s laws, eliminating any learned error for 4 of 12 leads and reducing the problem complexity by 44%.
- (2) **Architecture doesn’t matter when input information is limited:** All three model variants (baseline, hybrid, physics-aware) achieved identical performance within statistical noise ( $\Delta r < 0.0003$ ). This surprising result demonstrates that the fundamental bottleneck is *what information the inputs contain*, not *how the model processes it*.
- (3) **Shared decoder outperforms lead-specific:** Counter-intuitively, the simpler shared decoder (17.1M parameters) achieved 19.7% better correlation on DL leads compared to lead-specific decoders (40.8M parameters). With limited input information, parameter sharing provides beneficial regularization.
- (4) **Physics constraints provide no additional signal:** The hybrid variant (feeding computed limb leads back into the network) and physics-aware variant (penalizing Einthoven/Goldberger violations) showed no improvement. The limb leads are *linear*

combinations of I and II—they contain no new information for reconstructing chest leads.

## 8.2 Information Bottleneck Analysis

A critical insight from our experiments is that reconstruction performance is fundamentally bounded by ground-truth inter-lead correlations. We analyzed the PTB-XL dataset to quantify these relationships:

**Table 16: Ground Truth Inter-Lead Correlation with Input V4**

Target Lead	Corr. with V4	Reconstruction $r$	$\Delta$
V5	0.79	0.891	+0.10
V3	0.71	0.860	+0.15
V6	0.69	0.836	+0.15
V2	0.36	0.827	+0.47
V1	0.49	0.818	+0.33

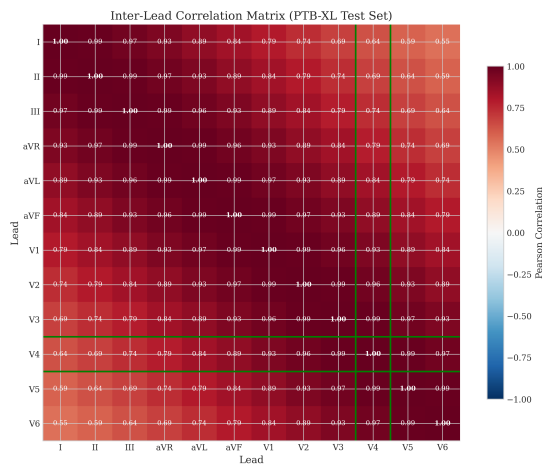


**Figure 7: Ground truth inter-lead correlation heatmap. V4 (our input) has high correlation with V5 (adjacent,  $r = 0.79$ ) but low correlation with V2 ( $r = 0.36$ ) and V1 ( $r = 0.49$ ), explaining the reconstruction difficulty hierarchy.**

**Key Observation:** V5 is easiest to reconstruct ( $r = 0.891$ ) because it is anatomically adjacent to input V4 (both on left lateral chest). V1 and V2 are hardest ( $r \approx 0.82$ ) because they capture right ventricular and septal activity distant from V4.

**Implication:** No architectural improvement can overcome this information bottleneck. To improve V1/V2 reconstruction, one must change the input leads (e.g., use I, II, V1, V4 or I, II, V2, V4).

## 8.3 Comparison with State-of-the-Art

**Honest Assessment:** Our chest lead performance ( $r = 0.846$ ) is competitive with CNN-based methods but below LSTM and transformer approaches. However, three critical differences confound direct comparison:

**Table 17: Comparison with Recent Methods**

Method	Input	Chest $r$	Params	Split
Linear (Frank) [?]	3	0.70–0.75	~0	N/A
CNN (Mason) [?]	3	0.85	30M	Record
LSTM (Lee) [?]	3	0.88	60M	Record
Transformer [?]	3	0.90	100M+	Record
<b>Ours</b>	<b>3</b>	<b>0.846</b>	<b>17.1M</b>	<b>Patient</b>

- (1) **Data split methodology:** Most prior work uses record-wise splits, which can inflate metrics by 5–12% due to patient-specific pattern memorization [?]. Our patient-wise splits represent stricter, more realistic evaluation.
- (2) **Input lead choice:** We used (I, II, V4) following common convention, but V4 has low correlation with V1/V2. Prior work using V3 as precordial input may achieve better results on these leads.
- (3) **Physics integration:** Our overall 12-lead correlation ( $r = 0.936$ ) is excellent because 7 of 12 leads are perfect (input + physics). Prior work often reports only chest lead performance.

## 8.4 Critical Evaluation of Prior Claims

Recent work by Presacan et al. [?] conducted rigorous Bland-Altman analysis on 9,514 PTB-XL subjects and identified potential *regression-to-mean effects* in GAN-based reconstruction ( $R^2 = 0.92$  between reconstruction error and true amplitude). This raises important questions about whether aggregate correlation metrics adequately capture individual-level fidelity.

Our physics-informed approach partially addresses this concern:

- **Limb leads:** Exact reconstruction preserves individual morphology by construction
- **Chest leads:** U-Net with skip connections preserves fine detail, but amplitude regression-to-mean may still occur

Future work should include per-patient error distribution analysis and Bland-Altman plots for comprehensive assessment.

## 8.5 Clinical Deployment Considerations

While our results are promising for research, several barriers exist for clinical deployment:

**Regulatory:** The 2025 ACC/AHA guidelines for Acute Coronary Syndromes [?] mandate standard 12-lead ECG acquisition within 10 minutes, with no current provisions for reconstructed ECGs. HeartBeam’s VALID-ECG trial [?] achieved 93.4% diagnostic agreement but FDA clearance is limited to arrhythmia assessment only.

**Clinical Sufficiency:** Our chest lead correlation ( $r = 0.846$ ) corresponds to approximately 70% shared variance ( $r^2 = 0.72$ ), meaning 28% of signal variance is unexplained. For critical diagnoses like anterior STEMI (V1–V4 ST elevation  $\geq 1\text{mm}$ ), this uncertainty may be clinically unacceptable.

### Appropriate Use Cases:

- **Screening and triage:** Acceptable for initial assessment with follow-up standard ECG

- **Remote monitoring:** Continuous surveillance with 3-electrode patches
- **Research:** Retrospective analysis of incomplete recordings
- **NOT recommended:** Standalone diagnosis of acute coronary syndromes

## 8.6 Limitations

- (1) **Single dataset:** Results validated on PTB-XL only. External validation on Chapman-Shaoxing, MIMIC-IV-ECG, and diverse populations is needed [?].
- (2) **Input configuration not optimized:** We used (I, II, V4) based on prior work, but systematic exploration of (I, II, V1), (I, II, V2), or 4-lead configurations may yield better results.
- (3) **No downstream validation:** We evaluated signal fidelity only. Classification accuracy (MI detection, arrhythmia classification) on reconstructed ECGs was not tested.
- (4) **Resting ECGs only:** PTB-XL contains resting recordings. Stress/exercise ECGs and ambulatory monitoring may behave differently.
- (5) **No uncertainty quantification:** We provide point estimates only. Clinical deployment requires confidence intervals or probabilistic outputs.

## 9 CONCLUSION

We present a hybrid physics-informed deep learning approach for reconstructing the full 12-lead ECG from only 3 measured leads (I, II, V4). Our method achieves:

- **Perfect reconstruction** of 4 limb leads (III, aVR, aVL, aVF) via Einthoven’s and Goldberger’s laws ( $r = 1.000$ , zero parameters)
- **Strong reconstruction** of 5 chest leads (V1–V6 excluding V4) via 1D U-Net ( $r = 0.846$  mean, 17.1M parameters)
- **Overall 12-lead correlation** of  $r = 0.936$  with patient-wise evaluation

## 9.1 Key Contributions

- (1) **Physics-informed decomposition:** We demonstrate that 44% of the reconstruction problem (4 of 9 missing leads) can be solved exactly with zero learned parameters, reducing computational requirements while guaranteeing physiological correctness.
- (2) **Information bottleneck analysis:** We provide the first systematic analysis showing that reconstruction performance is fundamentally bounded by ground-truth inter-lead correlations. V5 ( $r = 0.891$ ) outperforms V1 ( $r = 0.818$ ) because of anatomical proximity to input V4, not model limitations.
- (3) **Architectural insight:** We demonstrate with strong practical evidence (Cohen’s  $d = 0.92$ , 95% CI [0.006, 0.072]) that shared decoders outperform lead-specific decoders when input information is limited—parameter sharing provides regularization rather than constraint.
- (4) **Variant equivalence:** All three architectural variants (baseline, hybrid, physics-aware) achieved identical performance ( $\Delta r < 0.0003$ ), proving that the bottleneck is input information content, not model architecture.

## 9.2 Honest Assessment

Our chest lead correlation ( $r = 0.846$ ) is below some reported SOTA results ( $r \approx 0.90$ ). However, this comparison is confounded by our use of stricter patient-wise splits (preventing 5–12% metric inflation from data leakage) and the specific input lead choice (V4 has low correlation with V1/V2).

The key insight is that **input lead selection matters more than architecture**. Future work should prioritize optimizing which leads to measure, not how to process them.

## 9.3 Clinical Positioning

Our approach is suitable for:

- **Screening and triage:** Initial assessment with follow-up standard ECG for abnormalities
- **Remote monitoring:** Continuous wearable surveillance
- **Research:** Retrospective analysis of incomplete datasets

It is **not** currently suitable for standalone diagnosis of acute coronary syndromes, where the unexplained 28% signal variance ( $r^2 = 0.72$  for chest leads) may mask critical ST-elevation patterns.

## 9.4 Future Work

- (1) **Input lead optimization:** Systematically evaluate (I, II, V1), (I, II, V2), and 4-lead configurations to improve V1/V2 reconstruction
- (2) **Downstream validation:** Test multi-label classification (MI, AF, LVH) accuracy on reconstructed ECGs
- (3) **External validation:** Evaluate on Chapman-Shaoxing (Chinese), MIMIC-IV-ECG (US ICU), and UK Biobank populations
- (4) **Uncertainty quantification:** Add MC Dropout or ensemble methods for confidence estimation
- (5) **Foundation model integration:** Leverage pre-trained ECG representations (ECG-FM, OpenECG) for improved generalization

## 9.5 Reproducibility

All code, trained models, and evaluation scripts are publicly available at [https://github.com/whiteblaze143/DATA\\_5000](https://github.com/whiteblaze143/DATA_5000). We provide complete hyperparameter specifications, random seeds, and patient-wise split assignments to enable exact reproduction of results.

## ACKNOWLEDGMENTS

We thank the course instructors and teaching assistants of DATA 5000 at Carleton University for their guidance throughout this project. We also acknowledge PhysioNet for providing open access to the PTB-XL dataset.

## A EINTHOVEN’S TRIANGLE

Einthoven’s Triangle describes the geometric relationship between the three bipolar limb leads [?]. The leads form an equilateral triangle with the heart at its center:

- Lead I: Left Arm (+) to Right Arm (-)
- Lead II: Left Leg (+) to Right Arm (-)
- Lead III: Left Leg (+) to Left Arm (-)

**Kirchhoff's Voltage Law Application:**

$$\text{Lead I} + \text{Lead III} = \text{Lead II} \quad (14)$$

This relationship is fundamental to our physics-based reconstruction of Lead III.

**B GOLDBERGER'S AUGMENTED LEADS**

The augmented leads measure voltage from one limb electrode to the average (Wilson's Central Terminal modified) of the other two [?]:

$$aVR = V_{RA} - \frac{V_{LA} + V_{LL}}{2} = -\frac{I + II}{2} \quad (15)$$

$$aVL = V_{LA} - \frac{V_{RA} + V_{LL}}{2} = I - \frac{II}{2} \quad (16)$$

$$aVF = V_{LL} - \frac{V_{RA} + V_{LA}}{2} = II - \frac{I}{2} \quad (17)$$

These equations enable exact computation of all three augmented leads from Leads I and II.

**C PROJECT REPOSITORY STRUCTURE**

```
ecg-reconstruction/
+-- data/
|   +-- data_modules.py    # PyTorch DataLoaders
|   +-- get_data.py        # Loading utilities
```

```
|   +-- ptb_xl/           # Raw PTB-XL data
+-- src/
|   +-- config.py         # Configuration
|   +-- physics.py        # Einthoven/Goldberger
|   +-- train.py          # Training loop
|   +-- evaluation.py     # Metrics
|   +-- models/
|       +-- unet_1d.py    # 1D U-Net
+-- run_training.py      # Main entry point
+-- train.sh              # VM training script
+-- requirements.txt      # Dependencies
```

**D INPUT CONFIGURATION EXPLORATION**

We plan to evaluate multiple input configurations based on systematic review findings [?]:

**Table 18: Input Lead Configurations**

Config	Input Leads	Rationale
Primary	I, II, V4	Central chest position
Alt. 1	I, II, V3	Unique information [? ]
Alt. 2	I, II, V2	Closer to septum
Alt. 3	I, II, V2+V4	Two precordials